energies

MDPI

Article

Equivalent Modeling of LVRT Characteristics for Centralized DFIG Wind Farms Based on PSO and DBSCAN

Ning Zhou [1], Huan Ma [1], Junchao Chen [2], Qiao Fang [1], Zhe Jiang [1] and Changgang Li [2,*]

[1] Power Grid Technology Center, State Grid Shandong Electric Power Research Institute, Jinan 250003, China
[2] School of Electrical Engineering, Shandong University, Jinan 250061, China
* Correspondence: lichgang@sdu.edu.cn; Tel.: +86-135-7310-1895

Abstract: As large-scale wind turbines are connected to the grid, modeling studies of wind farms are essential to the power system dynamic research. Due to the large number of wind turbines in the wind farm, detailed modeling of each wind turbine leads to high model complexity and low simulation efficiency. An equivalent modeling method for the wind farm is needed to reduce the complexity. For wind farms with widely used doubly-fed induction generators (DFIGs), the existing equivalent studies mainly focus on such continuous control parts as electrical control. These methods are unsuitable for the low voltage ride through (LVRT) part which is discontinuous due to switching control. Based on particle swarm optimization (PSO) and density-based spatial clustering of applications (DBSCAN), this paper proposes an equivalent method for LVRT characteristics of wind farms. Firstly, the multi-turbine equivalent model of the wind farm is established. Each wind turbine in the model represents a cluster of wind turbines with similar voltage variation characteristics. A single equivalent transmission line connects all wind turbines to the power grid. By changing the terminal voltage threshold to enter LVRT, each equivalent turbine can be in different LVRT states. Secondly, an LVRT parameter optimization method based on PSO is used to obtain the dynamic parameters of the equivalent wind turbines. This method of parameter optimization is applicable to the equivalent of LVRT parameters. Thirdly, a clustering method based on DBSCAN is used to obtain suitable clusters of wind turbines. This clustering method can classify wind turbines with similar electrical distances into the same cluster. Finally, two examples are set up to verify the proposed method.

Keywords: doubly-fed induction generator; low voltage ride through; dynamic equivalence; particle swarm optimization; density-based spatial clustering of applications

Citation: Zhou, N.; Ma, H.; Chen, J.; Fang, Q.; Jiang, Z.; Li, C. Equivalent Modeling of LVRT Characteristics for Centralized DFIG Wind Farms Based on PSO and DBSCAN. *Energies* **2023**, *16*, 2551. https://doi.org/10.3390/en16062551

Academic Editor: Adrian Ilinca

Received: 11 December 2022
Revised: 10 February 2023
Accepted: 3 March 2023
Published: 8 March 2023

1. Introduction

As more and more attention has been paid to the development and utilization of renewable energy in recent years, the proportion of wind power generation in the power system continues to increase. The impact of wind power generation on power system security is also increasing [1]. For example, in the blackout accident in the UK on 9 August 2019 [2], an unexpected fault occurred suddenly, and many wind turbines were disconnected from the grid following the fault during the rapidly dynamic process. It resulted in a significant power shortage which eventually caused severe impacts and losses. Therefore, in power system dynamic research, it is necessary to perform accurate modeling of wind turbines to simulate the complex dynamic processes of the wind farm under faults [3].

Centralized wind power generation based on doubly-fed induction generators (DFIGs) is a widely used generation form [4,5]. The detailed modeling of DFIG wind turbines involves various parts, including electrical control, low voltage ride through (LVRT) control, generator-converter, pitch angle control, drive shaft, aerodynamics, etc. [6]. The structure of these models is very complicated. Moreover, due to the small capacity of the wind turbine, the number of DFIGs in centralized wind farms is usually very large [7]. Detailed

modeling of each wind turbine leads to high model complexity [8,9]. Moreover, it makes the simulation very inefficient.

In order to improve the simulation efficiency, a suitable equivalent method is needed to model the wind farm [10]. Single-turbine equivalent is the most commonly used method, which replaces the wind farm with a single equivalent wind turbine. The current studies on single-turbine equivalent mainly include coherency-based dynamic equivalent [11], rotor-side controller-based dynamic equivalent [12], and similar coherency equivalent [13], and weighted average equivalent [14]. The accuracy of the single-turbine equivalent method is high when the wind turbines are closely distributed and the dynamic responses of all wind turbines are similar [15]. However, when the dynamic response varies significantly from turbine to turbine, the dynamic response characteristics of the entire wind farm cannot be accurately expressed by only one equivalent wind turbine.

In order to further improve the equivalent accuracy of wind farms, some studies have used the multi-turbine equivalent method in [16–18]. These studies mainly consider the response characteristics of the continuous control parts of wind turbines, such as electrical control. Therefore, the dynamic characteristics can be fitted with high accuracy when the terminal voltage drop of the wind turbine due to faults is slight. However, when severe faults cause significant terminal voltage drops, the wind turbines need to switch from normal operation mode to LVRT mode. This switching control has significant discontinuous characteristics. In this case, the equivalent method mentioned above for continuous control cannot be applicable to the LVRT equivalent with discontinuous control characteristics.

On the other hand, clustering is very significant in multi-turbine equivalent methods. The selection of clustering indexes can directly affect the accuracy of the equivalent model [19]. The current clustering indexes can be divided into two main categories, the first one is objective environmental indexes, such as wind speed [20], wake effect model [21], etc.; the second category is the electrical characteristics of the wind turbine, such as the operating state [22] and power [23] of the turbine. The objective environmental data are easier to obtain but have strong volatility and uncertainty, while the electrical characteristics are more accurate in the subgroup results due to their controllability. The reasonable choice of clustering indexes can improve the accuracy of the equivalent model when targeting different specific problems.

In order to solve the equivalent problem of LVRT for centralized DFIG wind farms, this paper proposes an LVRT equivalent method based on particle swarm optimization (PSO) and density-based spatial clustering of applications (DBSCAN). The rest of the paper is organized as follows. The characteristic of the wind turbine LVRT model is analyzed in Section 2. A multi-turbine equivalent model structure is established and the equivalent static parameters are obtained in Section 3. Each wind turbine in the model represents a cluster of wind turbines with similar voltage variation characteristics. The LVRT parameters of the equivalent wind turbines are optimized by the PSO in Section 4. The cluster of the wind turbines is obtained by the DBSCAN in Section 5. Following this, three case studies are used to verify the effectiveness of the proposed method in Section 6, and conclusions are drawn in Section 7.

2. Characteristics of the Wind Turbine LVRT Model

2.1. The Basic Model of Wind Turbines

Taking the commonly used model of the wind turbine as an example, the relationship among the parts mentioned in the introduction is shown in Figure 1.

In Figure 1, I_{pcmd} is the current command for controlling active power; E_{qcmd} is the voltage command for controlling reactive power; P_{cmd} and Q_{cmd} are the active and reactive power commands.

The wind turbine determines whether to enter the LVRT mode based on the terminal voltage. When the terminal voltage drops and causes the wind turbine to enter the LVRT mode, both P_{cmd} and Q_{cmd} are controlled by the LVRT control model.

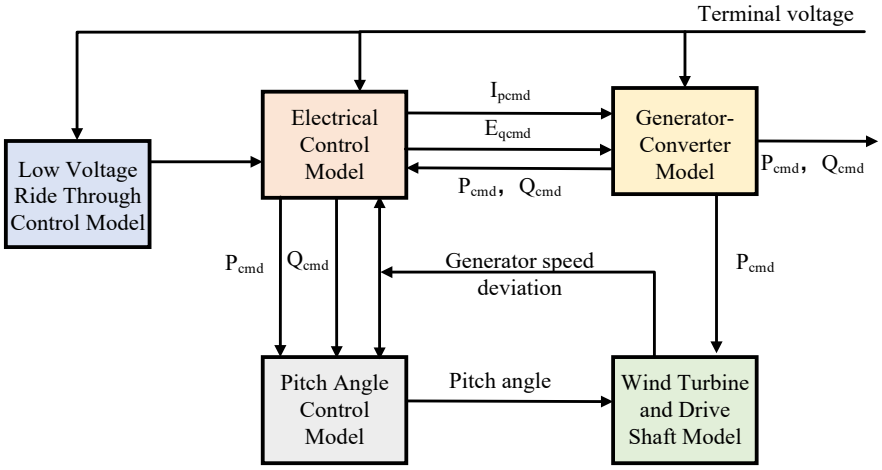

Figure 1. Relationship among the parts in the model of the wind turbine.

2.2. Analysis of the LVRT Control Model

The LVRT control models of the wind turbine in the current simulation software are similar with minor differences. The model of the Type 2 DFIG in the Power System Analysis Software Package (PSASP) developed by China Electric Power Research Institute is used in this paper. In terms of engineering practicality, PSASP is currently the most commonly used software in China for large-scale grid modeling studies. Therefore, PSASP was chosen as the simulation software in this paper in order to facilitate the application of the proposed equivalent method and the subsequent dynamic simulation analysis of the wind farm equivalent model. According to the wind turbine transient control characteristics, the PSASP designs a control method to simulate the power response characteristics of the wind turbine during the LVRT. The active power response of the wind turbine in the LVRT mode is shown in Figure 2.

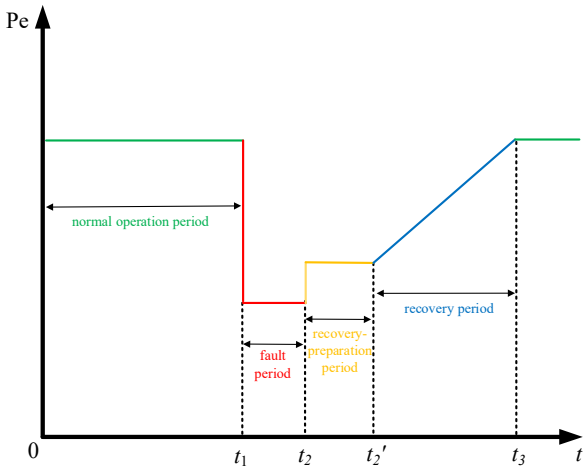

Figure 2. Active power response of LVRT control mode.

The LVRT control is divided into three periods, t_1~t_2 is the fault period of LVRT; t_2~t_2' is the recovery-preparation period; t_2'~t_3 is the recovery period. The LVRT control model of wind farms in the three periods is described as follows.

(1) fault period

Over this period, the active and reactive power is controlled by the current command, as shown in Equation (1):

$$\begin{cases} I_{\mathrm{pc}}^{\mathrm{F}} = I_{\mathrm{pset}} + K_{\mathrm{pI}} I_{\mathrm{p0}} + K_{\mathrm{pV}} V_t \\ I_{\mathrm{qc}}^{\mathrm{F}} = I_{\mathrm{qset}} + K_{\mathrm{qI}} I_{\mathrm{q0}} + K_{\mathrm{qV}} \left(V_{\mathrm{Lin}} - V_t \right) \end{cases} \tag{1}$$

where $I_{\mathrm{pc}}^{\mathrm{F}}$ and $I_{\mathrm{qc}}^{\mathrm{F}}$ are the active and reactive current commands during the fault period; I_{pset} and I_{qset} are two constants to adjust the $I_{\mathrm{pc}}^{\mathrm{F}}$ and $I_{\mathrm{qc}}^{\mathrm{F}}$; K_{pI} and K_{qI} are the coefficients which are related to the initial active and reactive current; I_{p0} and I_{q0} are the initial active and reactive currents; K_{pV} and K_{qV} are the coefficients which are related to the voltage; V_t is the terminal voltage of the wind turbine; V_{Lin} is the terminal voltage threshold for wind turbines to enter LVRT.

From the above equation in this period, it can be seen that the active current of the wind turbine decreases with the drop of the terminal voltage. Since the reactive current is controlled by the difference between the LVRT threshold and the terminal voltage, the reactive current increases when the terminal voltage drops.

(2) recovery-preparation period

Over this period, the LVRT of the wind turbine is in the preparation process for recovery. The active and reactive power control modes are based on the percentage of initial current, as shown in Equation (2):

$$\begin{cases} I_{\mathrm{pc}}^{\mathrm{P}} = \min(I_{\mathrm{prec}} + K_{Ip}^{\mathrm{P}} I_{\mathrm{p0}}, I_{\mathrm{p0}}) \\ I_{\mathrm{qc}}^{\mathrm{P}} = \min(I_{\mathrm{qrec}} + K_{Iq}^{\mathrm{P}} I_{\mathrm{q0}}, I_{\mathrm{q0}}) \end{cases} \tag{2}$$

where $I_{\mathrm{pc}}^{\mathrm{P}}$ and $I_{\mathrm{qc}}^{\mathrm{P}}$ are the active and reactive current commands at the start of the LVRT recovery; I_{prec} and I_{qrec} are the preset active and reactive currents; K_{Ip}^{P} and K_{Iq}^{P} are the initial active and reactive current coefficients.

Over this period, the power generated by the wind turbine increases to a constant value, which is usually less than the power in normal operating conditions. This is to prevent shocks caused by rapid power recovery from affecting the security of wind turbine devices.

(3) recovery period

At this period, the LVRT of the wind turbine is in the recovery process. The reactive current is not limited and can be quickly recovered to the normal level after the fault is cleared. The active current control mode in the recovery period is constant slope control, as shown in Equation (3):

$$\begin{cases} I_{\mathrm{pc}}^{\mathrm{R}} = I_{\mathrm{pc}}^{\mathrm{P}} + k_{\mathrm{Ipc}} \left(t - t_2{}' \right) \\ k_{\mathrm{Ipc}} = S_{\mathrm{n}} k_0 / S_{\mathrm{B}} \end{cases} \tag{3}$$

where k_{Ipc} is the active current slope during the LVRT recovery process; t is the current simulation time; $t_2{}'$ is the start time of the recovery period; S_{n} is the nameplate capacity of the wind turbine; k_0 is the control parameter of recovery slope; S_{B} is the reference capacity.

When the terminal voltage of the wind turbine drops below the LVRT threshold, the wind turbine enters the LVRT mode. It can be seen that when the LVRT period of the wind turbine is switched, the current control commands are significantly different. This switching control in LVRT mode has significant discontinuous characteristics, which makes the equivalent method based on the continuous controlled electrical model no longer applicable. Therefore, it is necessary to find an equivalent method of wind turbines considering the LVRT discontinuous characteristics.

3. Static Equivalent of Centralized Wind Farms

Considering that most centralized wind farms are built with similar wind turbines, the model structure and control mode of the turbines are almost the same. Therefore, this paper focuses on wind farms with the same turbine structure and control mode.

3.1. Wind Farm Equivalent Model

The topology of the equivalent model is shown in Figure 3. Each equivalent wind turbine G_{eqk} (k = 1, 2, . . . , n) in the model represents a cluster of original wind turbines. These equivalent turbines are connected to the external power system via an equivalent transmission line L_{eq} and an equivalent transformer T_{eq}. The equivalent transmission line and transformer impedance parameters are obtained through the static equivalent method discussed in Section 3.3. The buses between each equivalent wind turbine are connected via zero impedance lines L_1, L_2, etc.

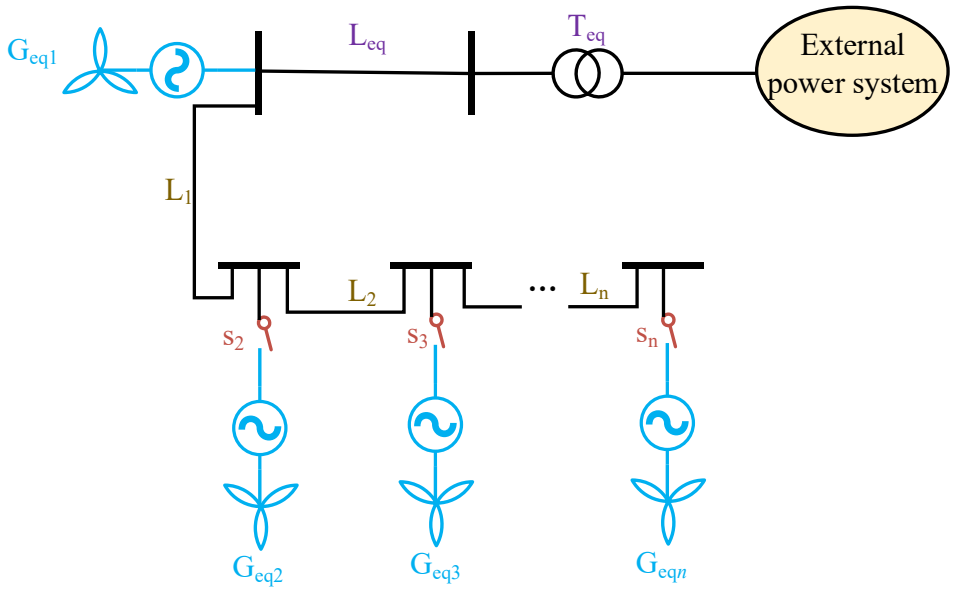

Figure 3. Wind farm equivalent model topology.

The switches (s_2, . . . , s_n) in the equivalent model control the connection and disconnection of the equivalent wind turbines. Therefore, this equivalent model can be applied to the multi-turbine equivalents. This model can also achieve a single-turbine equivalent when all switches are off. The different electrical distances from the fault location to the wind turbines lead to different terminal voltages strongly related to the LVRT characteristics, whereas in the multi-turbine equivalent model, the voltage of the bus connected to each wind turbine is the same because of the zero impedance lines. Therefore, the equivalent turbines cannot show the difference in the LVRT mode of wind turbines in the original wind farm due to the variation of the terminal voltage. This paper changes the terminal voltage threshold at which different wind turbines enter the LVRT mode to make the wind turbines at the same voltage express different LVRT states. The terminal voltage threshold variation is defined as ΔU in Equation (4):

$$\begin{cases} \Delta U = \overline{U} - U_0 \\ \overline{U} = \frac{\sum_{i=1}^{N_k} U_i}{N_k} \\ U_i^{\text{in}} = U_{\text{E}i}^{\text{in}} - \Delta U \\ U_i^{\text{out}} = U_{\text{E}i}^{\text{out}} - \Delta U \end{cases} \tag{4}$$

where $\overline{U}$ is the average value of the bus voltage of each wind turbine in the same cluster; U_0 is the bus voltage at the outlet of the wind farm; U_i is the bus voltage of each wind turbine in the same cluster; N_k is the number of wind turbines in the k-th cluster; k is the

number of clusters; U_i^{in} is the voltage at which the original wind turbine enters the LVRT mode; $U_{\text{E}i}^{\text{in}}$ is the voltage at which the equivalent wind turbine enters the LVRT mode; U_i^{out} is the voltage at which the original wind turbine exits the LVRT mode; $U_{\text{E}i}^{\text{out}}$ is the voltage at which the equivalent wind turbine exits the LVRT mode.

By changing the LVRT threshold of the equivalent wind turbine, the difference in the LVRT state of wind turbines in the original wind farm can be more accurately expressed. The accuracy of the equivalent wind farm can also be improved.

3.2. Wind Turbine Power and Nameplate Capacity Equivalent

The power and nameplate capacity of the equivalent wind turbine in the multi-turbine equivalent can be obtained by summing that of the original wind turbines within each cluster, as shown in Equation (5):

$$\begin{cases} S_{\text{neq}k} = \sum\limits_{i=1}^{N_k} S_{\text{n}i} \\ P_{\text{eq}k} = \sum\limits_{i=1}^{N_k} P_i \\ Q_{\text{eq}k} = \sum\limits_{i=1}^{N_k} Q_i \end{cases} \tag{5}$$

where $S_{\text{neq}k}$ is the nameplate capacity of the k-th equivalent wind turbine; k is the number of clusters; N_k is the total number of original wind turbines in the k-th cluster; $S_{\text{n}i}$ is the nameplate capacity of each original wind turbine in the k-th cluster; $P_{\text{eq}k}$ is the active power of the k-th equivalent wind turbine; P_i is the active power of each original wind turbine in the k-th cluster; $Q_{\text{eq}k}$ is the reactive power of the k-th equivalent wind turbine; Q_i is the reactive power of each original wind turbine in the k-th cluster.

When there is only one cluster, it is the single-turbine equivalent. In this case, the N_k is the number of all wind turbines in the original wind farm.

3.3. Transformer and Line Equivalent of the Wind Farm

Differences in transformer and line parameters between the original and the equivalent wind farm can impact the output power at the wind farm outlet and further lead to the inaccuracy of the equivalent result. Therefore, to improve the accuracy, the first step is to perform the static equivalent of the wind farm.

The equivalent transformer capacity is the sum of the capacity of each original transformer. The equivalent transformer impedance is calculated by using the weighted average method as shown in Equation (6):

$$\begin{cases} S_{\text{Teq}} = \sum\limits_{i=1}^{n_{\text{T}}} S_{\text{T}i} \\ Z_{\text{Teq}} = \sum\limits_{i=1}^{n_{\text{T}}} Z_{\text{T}i} S_{\text{T}i} / S_{\text{T}} \end{cases} \tag{6}$$

where S_{Teq} is the nameplate capacity of the equivalent transformer; $S_{\text{T}i}$ is the nameplate capacity of each original transformer; n_{T} is the total number of transformers in the original wind farm; Z_{Teq} is the impedance of the equivalent transformer; $Z_{\text{T}i}$ is the impedance of each original transformer; S_{T} is the sum of the capacities of all original transformers.

The method based on equivalent power loss is used to calculate the equivalent line impedance as shown in Equation (7):

$$Z_{\text{eq}} = \sum_{i,j=1}^{N} \left(Z_i {P_j}^2 \right) / \left(\sum_{j=1}^{N} P_j \right)^2 \tag{7}$$

where Z_i and Z_{eq} are the original impedance of the i-th line and equivalent impedance; P_j is the active power of the j-th original wind turbine; N is the total number of the original wind turbines.

4. PSO-Based LVRT Parameter Optimization Method

Because the equivalent researches on continuous control parts of wind turbines are already mature, the method in [24] is used to obtain the equivalent parameters of continuous control parts. In this paper, the focus of the equivalent of wind turbines is on the LVRT control parameters. The switching control of the LVRT leads to discontinuous characteristics. As an intelligent optimization algorithm, PSO is suitable for solving this discontinuous optimization problem. Therefore, this paper uses PSO to optimize the equivalent LVRT control parameters of wind turbines.

4.1. Basic PSO Algorithm

There is a particle swarm with m particles in a D-dimensional search space in the basic PSO. The i-th particle can be represented by a position vector $\boldsymbol{x}_i$ and a velocity vector $\boldsymbol{v}_i$, where $\boldsymbol{x}_i = (x_{i1}, x_{i2}, \ldots, x_{iD})$ $\boldsymbol{v}_i = (v_{i1}, v_{i2}, \ldots, v_{iD})$. The spatial position of the particles is a set of LVRT control parameters. The fitness can be calculated by the optimization objective function and can measure the merit of the solution. The particle position and velocity are updated according to the best historical fitness of the individual and the best global fitness of the whole. The next iteration is performed until the fitness is almost no longer changing or the number of iterations reaches the maximum. The evolution update process of each particle is shown in Equations (8) and (9):

$$v(m) = r_1\lambda_g\left(x_g - x(m-1)\right) + r_2\lambda_u(x_{ui} - x(m-1)) + \omega v(m-1) \tag{8}$$

$$x(m) = v(m) + x(m-1) \tag{9}$$

where m is the number of iterations; r_1 and r_2 are random numbers uniformly distributed within [0, 1]; λ_g and λ_u are global acceleration coefficients and individual acceleration coefficients; x_g is the position vector of the particle corresponding to the best global fitness; x_{ui} is the position vector corresponding to best historical fitness of the i-th particle; ω is the inertia coefficient.

The initial position of a single particle in a particle swarm is a multidimensional vector. The initial position of the particle swarm is defined as $\boldsymbol{X}_0 = [\boldsymbol{x}_1, \boldsymbol{x}_2, \ldots, \boldsymbol{x}_m]^{\mathrm{T}}$, where the position of the i-th particle is $\boldsymbol{x}_i = [x_1, x_2, \ldots, x_m]^{\mathrm{T}}$. In order to determine whether the PSO converges, the fitness of each particle needs to be calculated. The particle swarm fitness vector is defined as $\boldsymbol{F} = [F_1, F_2, \ldots, F_m]$, where F_i denotes the fitness of the i-th particle and is calculated by Equation (10):

$$F_i = \int_{t_a}^{t_b} \left\{ \left[\left(P_{pre} - P_{eq}\right)^2 + \left(Q_{pre} - Q_{eq}\right)^2 \right] \right\} \tag{10}$$

where P_{pre} and P_{eq} are the active powers at the outlet of the original and equivalent wind farm; Q_{pre} and Q_{eq} are the reactive powers at the outlet of the original and equivalent wind farm; t_a and t_b are the time when the wind turbine enters and exits the LVRT mode.

4.2. The Improvements of PSO

There are two main factors affecting the accuracy of PSO optimization, including the generation of initial particles and the setting of parameters in the evolutionary strategy. For the first factor, the initial position of LVRT control parameters in each particle will impact the search range of PSO. Therefore, a reasonable selection of the initial position is needed to improve the probability of the algorithm searching for the optimal solution. For the other factor, the inertia coefficient in the basic PSO is fixed in the iterative process, which makes the convergence of the algorithm slow and may cause the results to fall into the optimal local solution. Therefore, the PSO is improved in the above two aspects.

(1) Improvement of initial particles generation

This paper uses the method of generating reference points by weighted averaging to narrow down the generation of the initial particle population. Therefore, the particles are searched around the more reasonable initial LVRT control parameters to improve the search efficiency of PSO. In the case of single-turbine equivalent, the initial LVRT control parameters are calculated as shown in Equation (11):

$$x_{j0} = \sum_{i=1}^{N_k} x_{ji} S_i / S_{\mathrm{eq}k} \tag{11}$$

where x_{j0} is the weighted average of the j-th parameter ($j = 1, \ldots, p$); p is the total number of parameters; x_{ji} is the the j-th parameter of the i-th wind turbine in the k-th cluster; S_i is the nameplate capacity of the i-th wind turbine in the k-th cluster; $S_{\mathrm{eq}k}$ is the nameplate capacity of the k-th equivalent wind turbine, and N_k is the total number of wind turbines in the k-th cluster.

(2) Improvement of inertia coefficient

This paper balances the global search ability and local search ability of the PSO by changing the value of the inertia coefficient in the iterative process. The updated equation of the inertia coefficient is shown in Equation (12):

$$\omega = \begin{cases} \omega_{\min} - \frac{(\omega_{\max} - \omega_{\min})(F - F_{\min})}{F_{\mathrm{avg}} F_{\min}}, & F \le F_{\mathrm{avg}} \\ \omega_{\max}, & F > F_{\mathrm{avg}} \end{cases} \tag{12}$$

where $\omega_{\max}$ and $\omega_{\min}$ represent the maximum and minimum inertia weights, respectively; F represents the current fitness of the particle; F_{avg} represents the current average fitness of the particle; $F_{\min}$ represents the minimum fitness of the particle.

This method dynamically adjusts the inertia coefficient by comparing the current fitness with the average fitness in the iteration to achieve the balance between the global search ability and local search ability. Through this method, the equivalent accuracy and PSO convergence speed are improved.

5. Wind Turbines Clustering

5.1. Clustering Indicators

In the multi-turbine equivalence method for wind farms, it is first necessary to cluster the wind turbines. The impact on the LVRT characteristics of the wind turbine when a fault occurs in the power system is mainly achieved by affecting the terminal voltage of the turbine. Therefore, this paper divides wind turbines with similar voltage drops into the same cluster. In this way, the LVRT characteristics of wind turbines in the same cluster change similarly.

The electrical distance which is from the installed position of the wind turbine to the fault location can affect the terminal voltage of the wind turbine. Therefore, the electrical distance of the wind turbines is considered a clustering indicator. The turbines within the same cluster have similar voltage drops and dynamic characteristics.

The impedance method is used to get the electrical distance. The system impedance matrix is obtained by the node admittance matrix. The electrical distance matrix is calculated from the elements in the impedance matrix, as shown in Equation (13):

$$d_{ij} = z_{ii} - z_{ij} + z_{jj} - z_{ji} \tag{13}$$

where d_{ij} is the electrical distance between the i-th and j-th nodes; z_{ii} and z_{jj} are the self-impedances of the i-th and j-th nodes, respectively; z_{ij} and z_{ji} are the mutual impedances of the i-th and j-th nodes.

5.2. The Clustering Method Based on DBSCAN

The current clustering methods are divided into two main categories: those that require and those that do not require specifying the number of clusters in advance. Because a reasonable number of wind turbine clusters cannot be determined in advance, this paper chooses the DBSCAN clustering method [25]. DBSCAN does not need to determine the number of clusters in advance but speculates the number of clusters based on the data. Moreover, it is a density-based clustering method which is suitable for wind turbine clustering problems based on the electrical distance. However, the traditional DBSCAN algorithm first needs to determine two parameters artificially. One is the E, the radius of the proximity region around a point. The other is the $C_{\min}$, the number of electrical distance points contained at least in the proximity region. The choice of these two parameters directly determines the clustering effect. Since these two parameters also cannot be specified artificially before clustering, the traditional DBSCAN is improved in this paper to determine the optimal parameters E and $C_{\min}$ adaptively.

The improved DBSCAN is mainly based on the parameter-finding strategy. It uses the distribution characteristics of the electrical distance data to generate the candidate E and $C_{\min}$. Then, it can automatically find the appropriate number of clusters and obtain the corresponding parameters. The specific calculation process of the improved DBSCAN is shown in Figure 4.

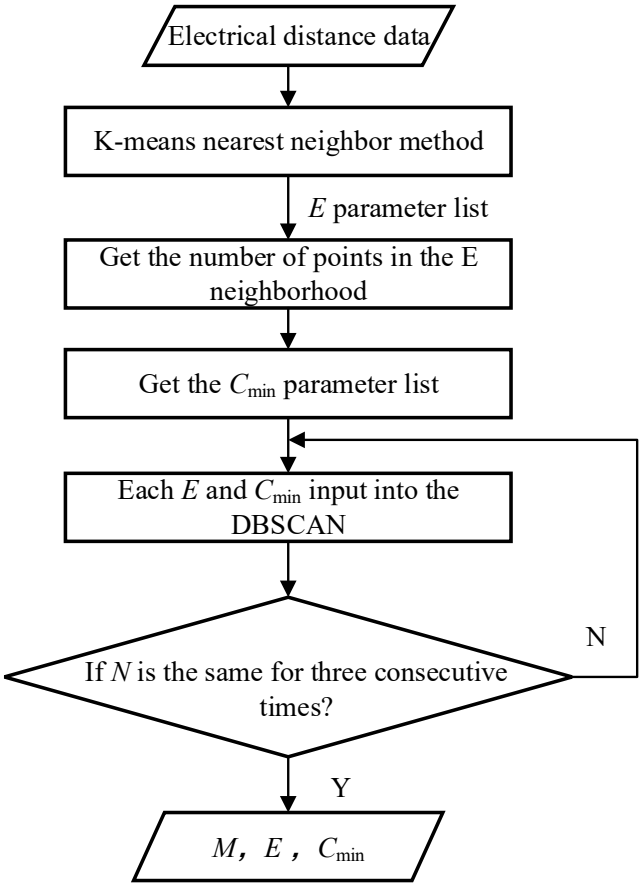

Figure 4. Process of the improved DBSCAN.

First, the k-nearest neighbor algorithm is used to generate the list of E. Then, iterate through each E to determine the number of points in the neighborhood of E. Then the $C_{\min}$ is calculated according to Equation (14) to obtain the list of $C_{\min}$:

$$C_{\min} = \left(\sum_{i=1}^{a} C_i\right)/a \tag{14}$$

where C_i is the number of points in the E neighborhood of the i-th point, and a is the total amount of data.

The elements in the list of E and the elements in the corresponding list of $C_{\min}$ are selected and input into the DBSCAN to get the M which is the number of clusters. The clustering result converges when the number is the same for three consecutive times. At this time, the M is the optimal number of clusters. The E and $C_{\min}$ corresponding to the M are the optimal parameters to achieve the adaptive determination of parameters in the DBSCAN.

It should be noted that the real and imaginary parts of the electrical distance data of each wind turbine are used as x and y coordinates to obtain the data used for clustering. They then apply adaptive DBSCAN to the processed data to achieve clustering of wind turbines. The DBSCAN uses the Euclidean distance between the points in the processed data as the specific clustering indicator, as shown in Equation (15):

$$\rho_i = \sqrt{(x_i - x_j)^2 + (y_i - y_j)^2} \tag{15}$$

where ρ_i is the Euclidean distance between two points in the data; x_i and x_j are the x coordinates of the i-th and j-th point in the processed electrical distance data; y_i and y_j are the y coordinates of the i-th and j-th point in the processed electrical distance data.

6. Verification of the Equivalent Method

6.1. Test System

The structure of the original centralized DFIG wind farm in the test system is shown in Figure 5. There are two main collector lines in the original wind farm, each connecting ten wind turbines. The parameters of wind turbines are different, and some of them are shown in Tables 1 and 2. The external power system is simulated with an ideal infinity generator. It is connected to the bus at the wind farm outlet via the transmission line and the transformer.

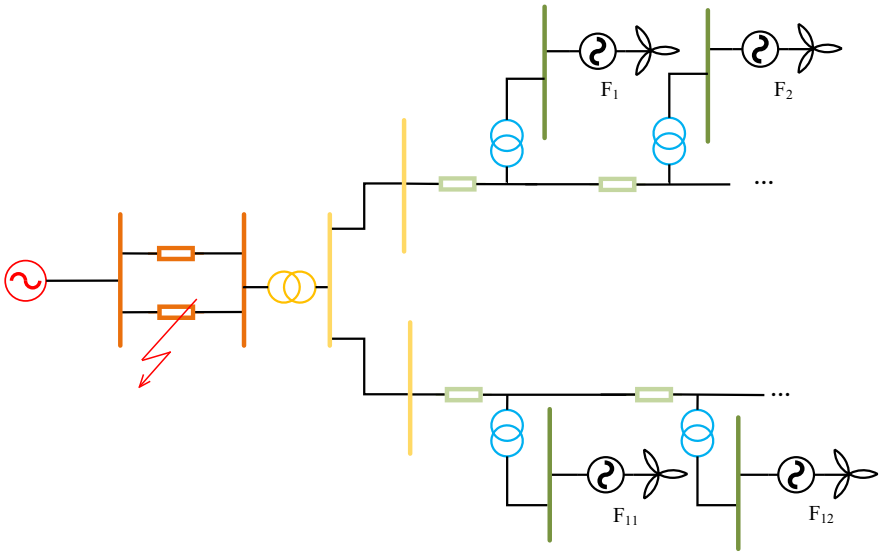

Figure 5. The structure of the original wind farm.

Table 1. The operating status of some wind turbines in the original wind farm.

	F1	F3	F5	F7	F9	F11	F13
P (MW)	2.13	2.06	1.99	1.87	1.82	2.16	2.00
Q (MVar)	0.43	0.40	0.35	0.32	0.29	0.45	0.43

Table 2. The LVRT control parameters of different wind turbines in the original wind farm.

	K_{pV}	K_{qV}	I_{pset} (p.u.)	I_{qset} (p.u.)	K_{Ip}^{P}	K_{Iq}^{P}	K_{pI}	K_{qI}	I_{prec} (p.u.)	I_{qrec} (p.u.)	k
F1	0.00	0.00	0.00	0.00	0.36	0.00	0.00	30.90	0.00	0.00	1.00
F5	0.53	1.52	0.00	0.00	1.00	−0.20	0.50	1.00	0.00	0.00	1.00
F11	0.00	1.21	0.21	0.10	0.58	0.00	0.25	2.50	0.40	0.10	1.00
F15	0.48	1.00	0.35	0.10	0.24	0.00	0.25	2.50	0.80	0.10	1.00

In this paper, different faults are set up to make the terminal voltage of the wind farm drop to various levels. The specific fault in the simulation is a three-phase short-line fault. The grounding impedance of different faults is set as (p.u.): $Z_{f1} = 0 + j0.2$, $Z_{f2} = 0 + j0.4$, $Z_{f3} = 0 + j0.6$, $Z_{f4} = 0 + j0.3$, $Z_{f5} = 0 + j0.5$ and $Z_{f6} = 0 + j0.7$.

6.2. Case Study 1: Single Turbine Equivalent under the Close Distribution of Wind Turbines

Case study 1 considers the situation that the wind turbines in the wind farm are relatively closely connected. That is, the installed positions of each wind turbine are relatively close. The specific line lengths are shown in Table 3. In this table, L_{ij} represents the length between the i-th wind turbine and the j-th wind turbine in the wind farm.

Table 3. Length of lines between different wind turbines in the original wind farm in Case study 1.

Line	$L_{1,2}$	$L_{2,3}$	$L_{3,4}$	$L_{4,5}$	$L_{5,6}$	$L_{6,7}$	$L_{7,8}$	$L_{8,9}$	$L_{9,10}$
Length (km)	0.4	0.4	0.4	0.6	1.2	0.4	0.4	0.4	0.4
Line	$L_{11,12}$	$L_{12,13}$	$L_{13,14}$	$L_{14,15}$	$L_{15,16}$	$L_{16,17}$	$L_{17,18}$	$L_{18,19}$	$L_{19,20}$
Length (km)	0.4	0.4	0.4	0.5	0.4	0.6	0.4	0.8	0.4

First, the number of equivalent wind turbines needs to be determined. The electrical distance of each wind turbine in the wind farm is shown in Figure 6. By applying the improved DBSCAN, the number of clusters and the corresponding parameters are $M = 1$, $E = 0.64$, and $C_{min} = 18$. Due to the dense distribution of wind turbines in this centralized wind farm, the wind turbines are only divided into one cluster. An equivalent wind turbine is used to perform the characteristics of the wind farm.

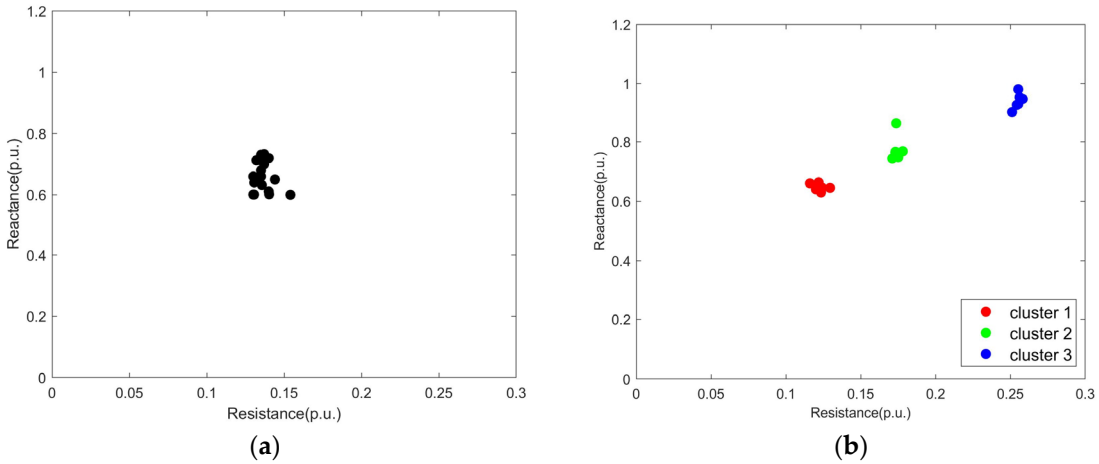

Figure 6. Distribution of wind turbine electrical distance. (**a**) Case study 1. (**b**) Case study 2.

The improved PSO can be used to obtain the parameters of the equivalent wind turbine under faults Z_{f1}, Z_{f2}, and Z_{f3}. In order to further verify the generality of the parameters, the obtained equivalent wind turbine is simulated again under faults Z_{f4}, Z_{f5}, and Z_{f6}. The results of comparing the active and reactive power at the outlet of the original and equivalent wind farm are shown in Figure 7.

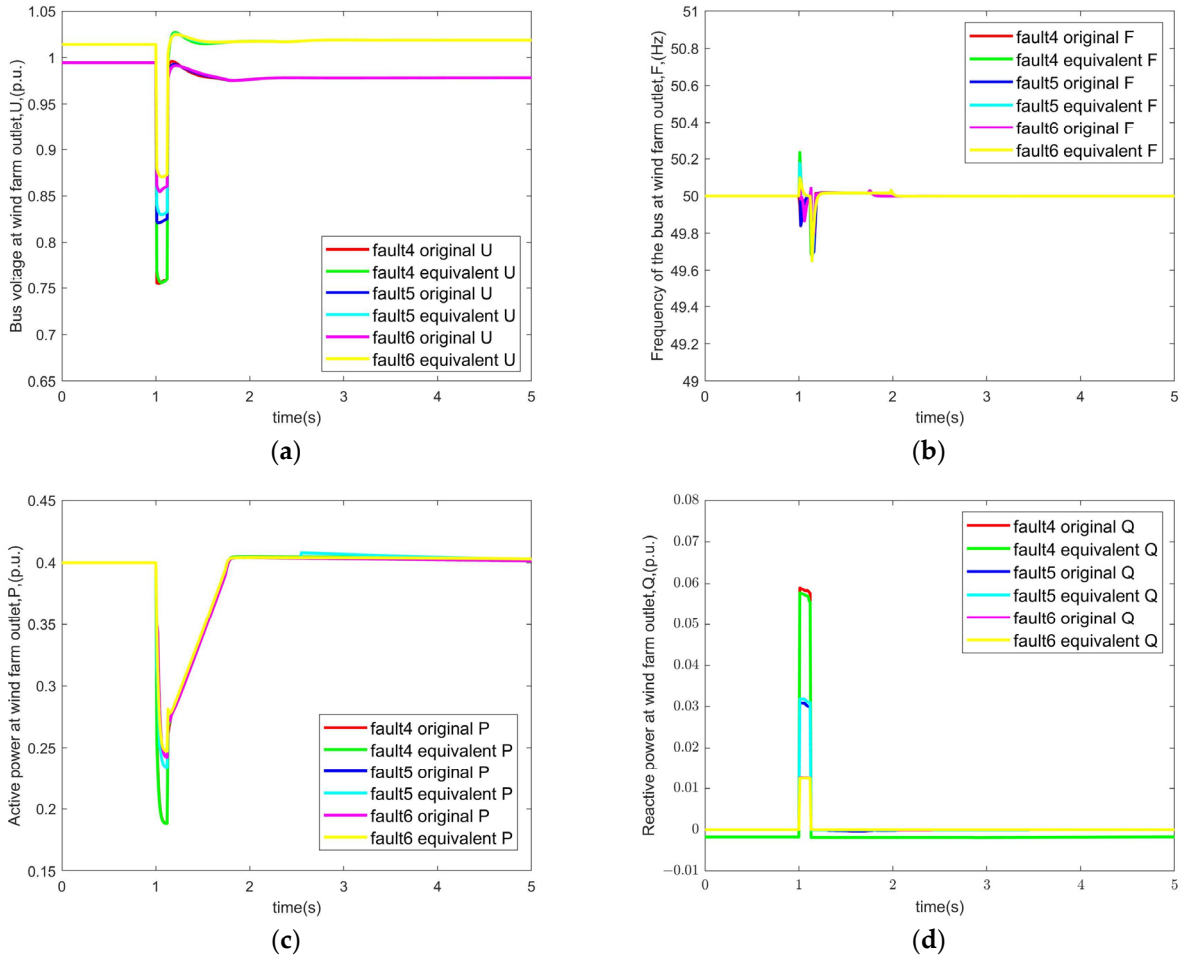

Figure 7. Equivalent results of Case study 1. (**a**) Terminal voltage. (**b**) Active power. (**c**) Reactive power. (**d**) Frequency.

From the results, it can be seen that the initial terminal voltage of the equivalent system differs from the original system before the fault occurs, which is caused by the static equivalence error of the wind farm. Throughout the equivalence process, the bus frequency fluctuations at the wind farm outlet are relatively small and cannot lead to serious grid failures. For active power, the LVRT control of the wind turbine is recovered with a constant starting point and slope during the recovery phase. Therefore, the active power dips at different levels under different faults, but the curve of the recovery process is the same.

In this paper, the accuracy of the equivalent is evaluated by calculating the root mean square error (RMSE) of the power between the original and the equivalent system. Under three different faults, the RMSE of the active and reactive power are 3.3% and 1.2%. These errors are allowable in engineering research.

To verify the superiority of the proposed method in this paper, the weighted average method and the basic PSO method are applied to this case study under the fault Z_{f4} and the equivalent results are compared as shown in Figure 8.

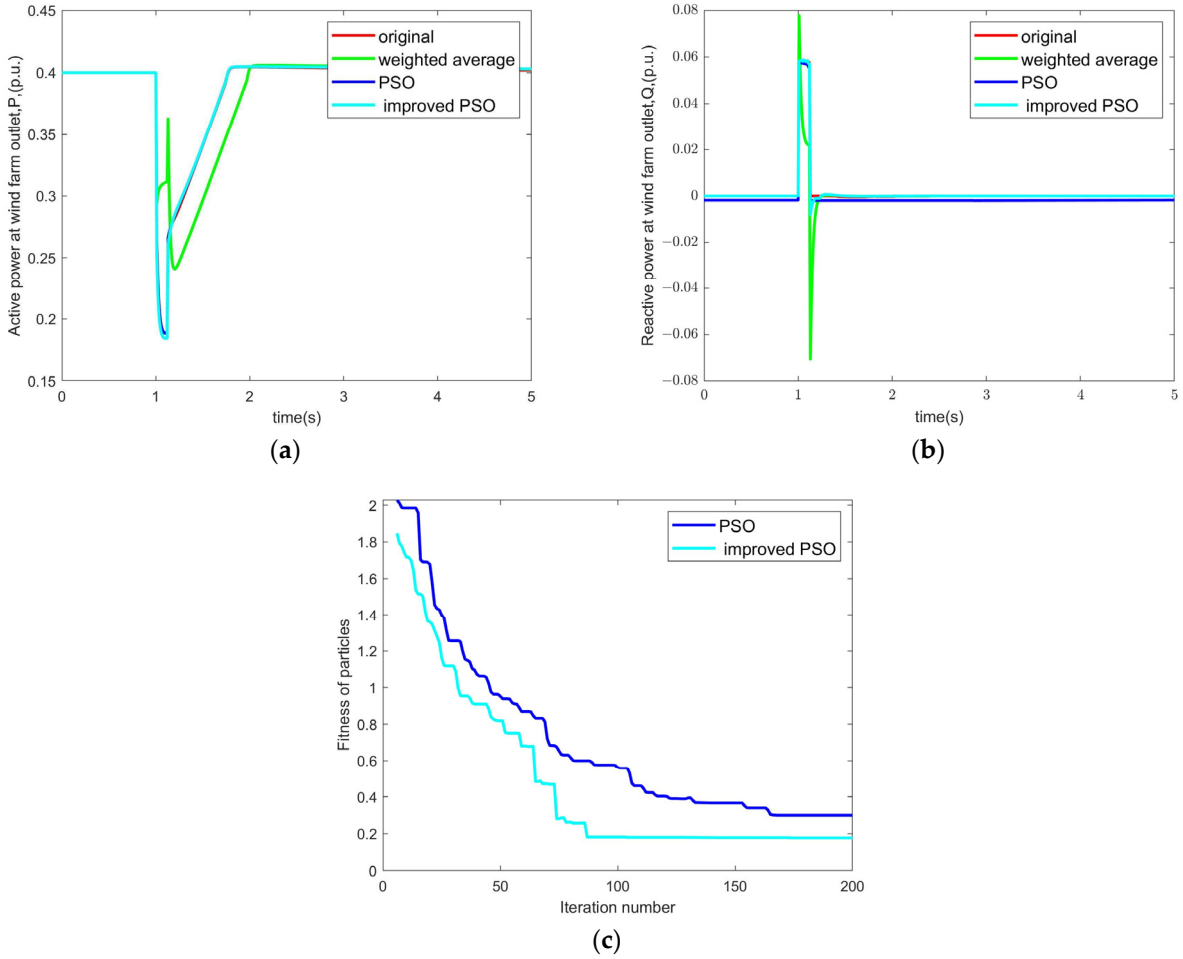

Figure 8. Comparison of different methods. (**a**) Active power. (**b**) Reactive power. (**c**) Convergence speed.

Under three different methods, the RMSE of the active and reactive power are shown in Table 4.

Table 4. The RMSE under different methods.

Method	The RMSE of P (%)	The RMSE of Q (%)
Weighted Average	24.08	10.86
Basic PSO	1.85	3.36
Improved PSO	1.26	1.98

The comparison shows that the equivalent results obtained by the weighted average method are not satisfactory when there are differences in wind turbine parameters within the wind farm. This is mainly due to the fact that the weighted averaging changes the control parameters of the LVRT recovery period, which makes the power of the equivalent turbines during the fault recovery vary significantly. Although the basic PSO method has higher equivalence accuracy, its convergence speed is slow. It can be seen from (c) that the improved PSO has 40.5% fewer iterations than the basic PSO, and the best fitness of the improved PSO is improved by 6.1%. This indicates that the improved PSO proposed in this paper has higher equivalent accuracy and convergence speed.

As mentioned above, when the distribution of wind turbines is close to each other, the equivalent of wind farms can be achieved with only one wind turbine. The results show that the equivalent of the original system is achieved with high accuracy, which proves the effectiveness of the equivalent method in this paper.

6.3. Case Study 2: Multi-Turbine Equivalent under the Decentralized Distribution of Wind Turbines

Considering that the installed locations of wind turbines in wind farms may be scattered due to the terrain, the terminal voltage drop of the wind turbines in different locations is various. At this time, one equivalent wind turbine cannot simulate the dynamic characteristics of the wind farm. The wind farm needs to be clustered to achieve the multi-turbine equivalent.

In Case study 2, different line impedance is set to simulate the installed positions of the wind turbines. The specific lengths are shown in Table 5. The electrical distances of each wind turbine are shown in Figure 6. The improved DBSCAN is applied to obtain the number of clusters. The corresponding parameters are $M = 3$, $E = 0.27$, and $C_{\min} = 5$. The specific wind turbine clustering result is shown in Table 6.

Table 5. Length of lines between different wind turbines in the original wind farm in Case study 2.

Line	$L_{1,2}$	$L_{2,3}$	$L_{3,4}$	$L_{4,5}$	$L_{5,6}$	$L_{6,7}$	$L_{7,8}$	$L_{8,9}$	$L_{9,10}$
Length (km)	0.4	0.4	0.4	0.44	0.4	2.4	0.4	2.8	0.4
Line	$L_{11,12}$	$L_{12,13}$	$L_{13,14}$	$L_{14,15}$	$L_{15,16}$	$L_{16,17}$	$L_{17,18}$	$L_{18,19}$	$L_{19,20}$
Length (km)	0.4	2.4	0.4	0.4	0.4	0.6	2.8	0.4	0.4

Table 6. The clustering result of wind turbines in Case study 2.

Cluster Number	**Turbine Number**
1	F1, F2, F3, F4, F5, F6, F11, F12
2	F7, F8, F13, F14, F15, F16
3	F9, F10, F17, F18, F19, F20

In order to verify that the results of the multi-turbine equivalent are more accurate than the single-turbine equivalent, the simulation results under faults Z_{f1}, Z_{f2}, and Z_{f3} are obtained to perform the single-turbine and multi-turbine equivalent. Then, the obtained single-turbine and multi-turbine equivalent models and the original wind farm model are further simulated and analyzed under faults Z_{f4}, Z_{f5}, and Z_{f6}. The results of comparing the active and reactive power at the original and equivalent wind farm outlet are shown in Figures 9–11.

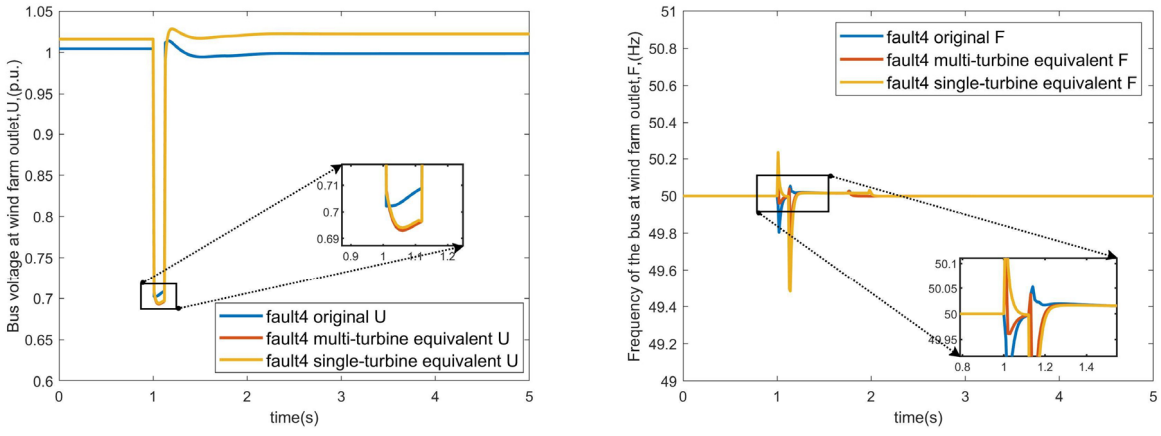

(**a**) (**b**)

Figure 9. *Cont.*

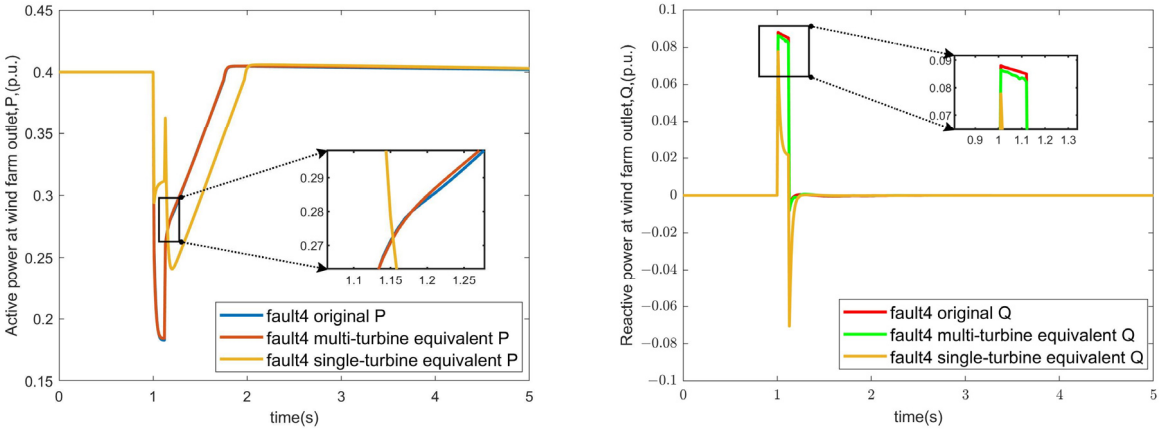

(**c**) (**d**)

Figure 9. Equivalent results of Case study 2 under fault 4. (**a**) Terminal voltage. (**b**) Active power. (**c**) Reactive power. (**d**) Frequency.

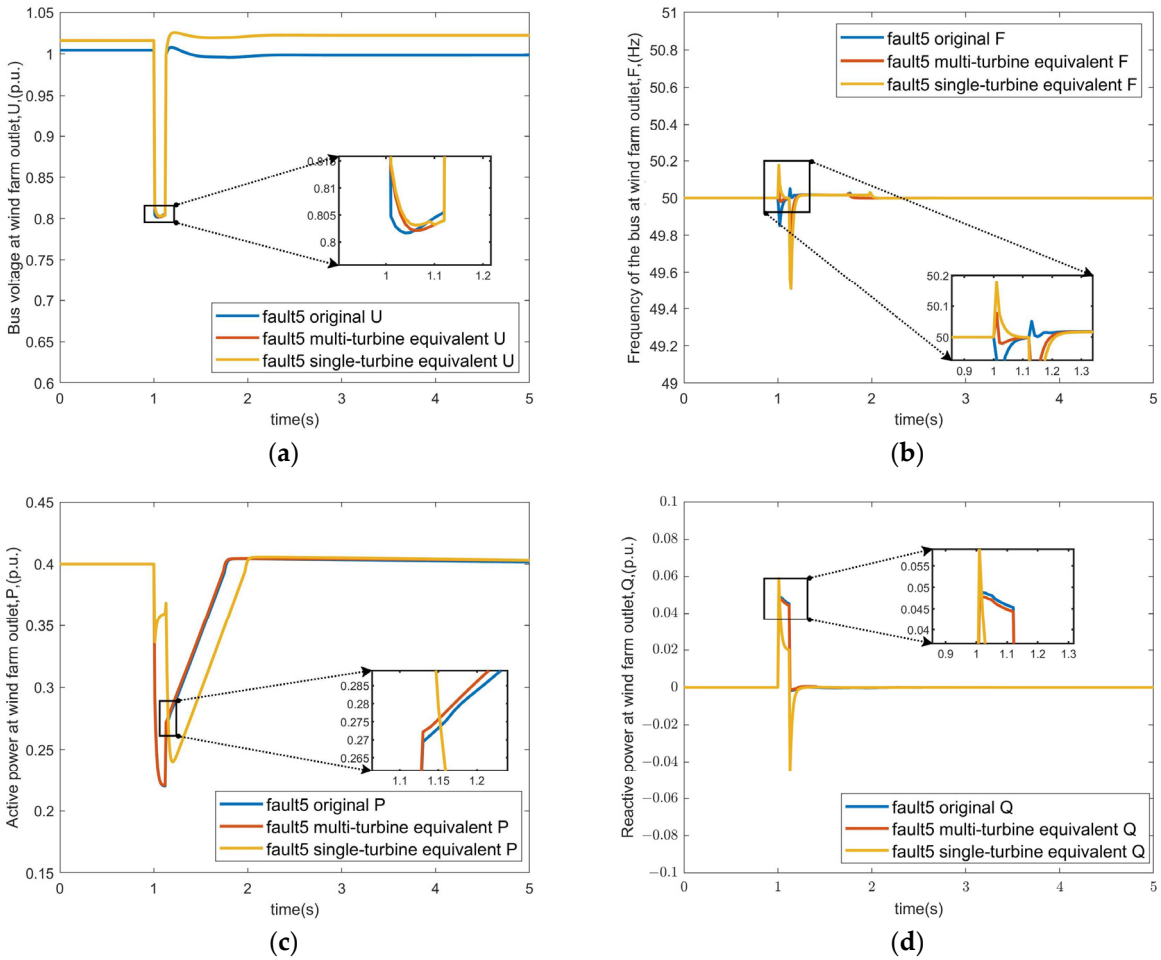

(**a**) (**b**)

(**c**) (**d**)

Figure 10. Equivalent results of Case study 2 under fault 5. (**a**) Terminal voltage. (**b**) Active power. (**c**) Reactive power. (**d**) Frequency.

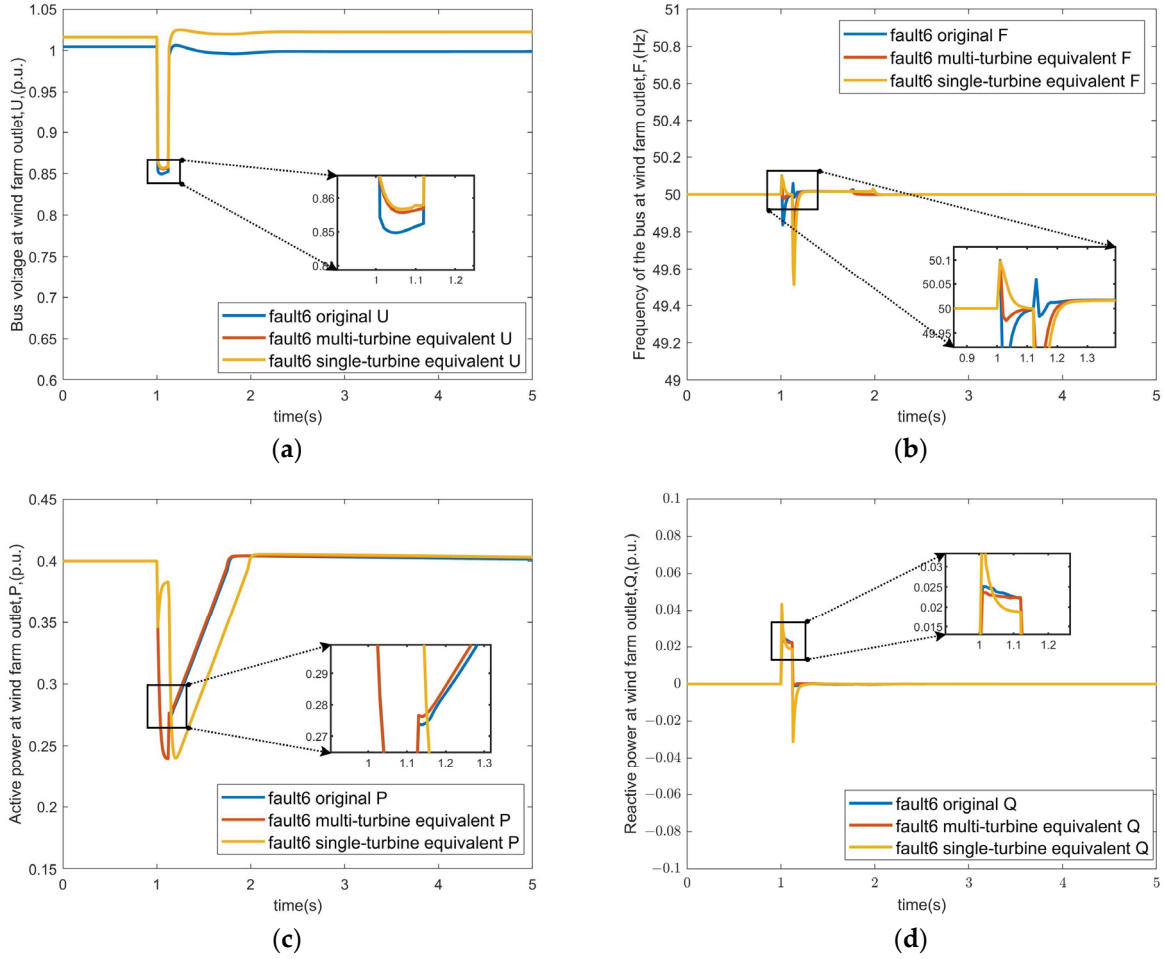

Figure 11. Equivalent results of Case study 2 under fault 6. (**a**) Terminal voltage. (**b**) Active power. (**c**) Reactive power. (**d**) Frequency.

The above results show that the terminal voltage of the equivalent model before the fault is different from the original wind farm due to the static equivalent error of the wind farm. However, the drops in terminal voltage during the faults is similar, so this terminal voltage difference has a small impact on the equivalent accuracy. During the whole equivalence process, the fluctuation of the bus frequency at the wind farm outlet is small and cannot cause serious grid faults.

For the active power of the wind turbine, the difference between the multi-turbine equivalent and single-turbine equivalent results is mainly concentrated in the recovery period of the LVRT. This is due to the fact that the LVRT recovery process of wind turbines under different voltage drops in a wind farm varies. A wind turbine can only show one of the LVRT recovery states, and cannot show the impact on the wind farm when different LVRT states are superimposed.

The RMSE of the active and reactive power is 20.25% and 12.86%, respectively, in the single-turbine equivalent. In comparison, those in the multi-turbine equivalent are 1.12% and 2.06%, respectively. The results show that the single-turbine equivalent model cannot fully represent the LVRT dynamic characteristics of the original wind farm. In contrast, after reasonable clustering, the multi-turbine equivalent can perform the characteristics of LVRT and have higher accuracy than the single-turbine equivalent.

6.4. Case Study 3: Multi-Turbine Equivalent under the Large Capacity Wind Farms

To verify the applicability of the equivalent method proposed in this paper in large capacity wind farms, Case study 3 uses an actual wind farm in China. The specific wind

farm structure and distances are shown in Figure 12. The parameters of wind turbines are different, and some of them are shown in Tables 7 and 8.

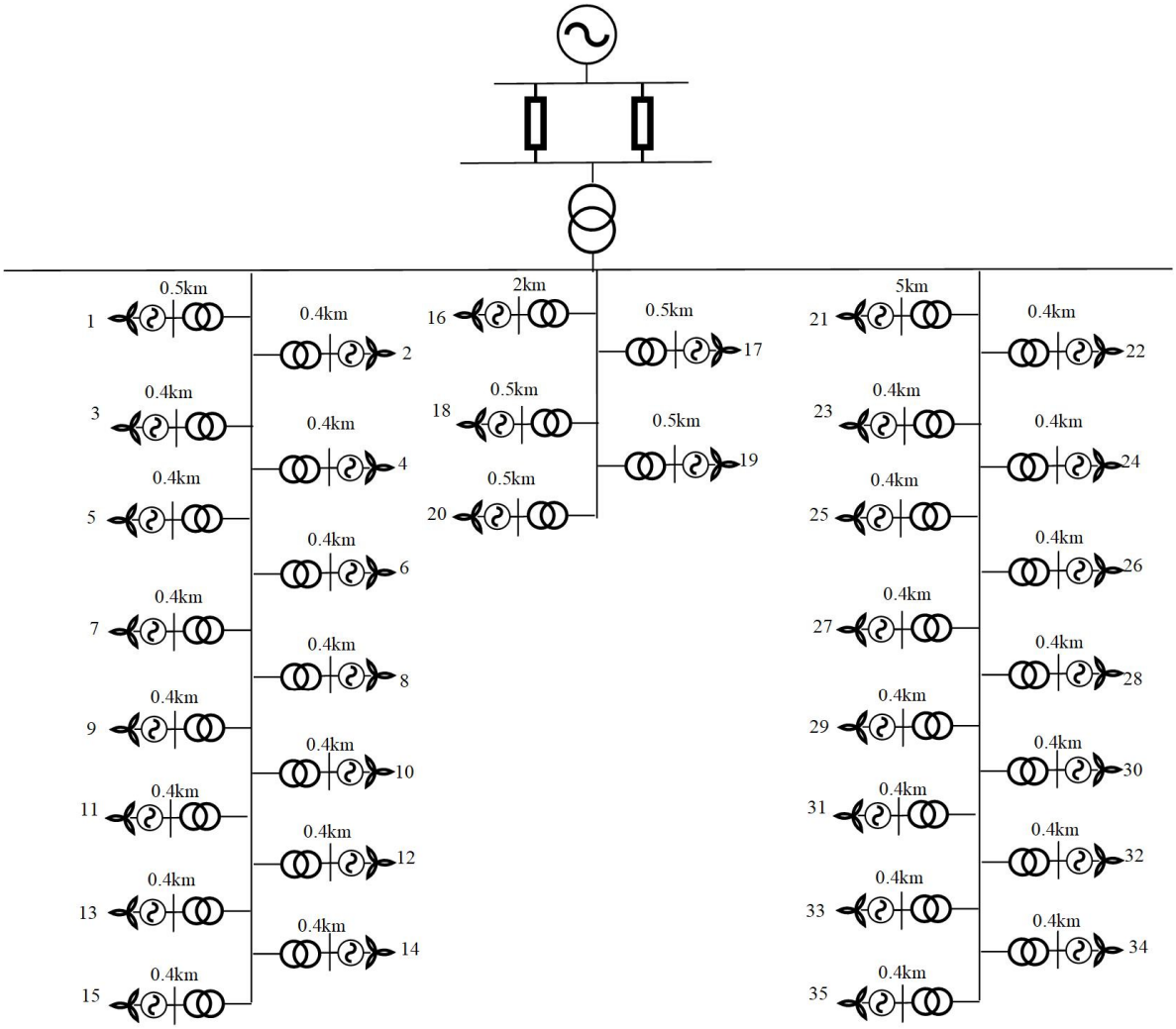

Figure 12. The structure of the original wind farm with large capacity.

Table 7. The operating status of some wind turbines in the original large capacity wind farm.

	1	**5**	**10**	**15**	**16**	**19**	**20**	**25**	**30**	**35**
P (MW)	2.51	2.55	2.49	2.46	2.53	2.50	2.49	2.51	2.50	2.52
Q (MVar)	0.55	0.48	0.42	0.40	0.53	0.50	0.48	0.47	0.45	0.42

Table 8. The LVRT control parameters of different wind turbines in the original large capacity wind farm.

	K_{pV}	K_{qV}	I_{pset} (p.u.)	I_{qset} (p.u.)	K_{Ip}^{P}	K_{Iq}^{P}	K_{pI}	K_{qI}	I_{prec} (p.u.)	I_{qrec} (p.u.)	k
1	0.50	1.03	0.00	0.00	0.76	1.73	0.50	1.00	0.20	0.10	1.00
16	0.53	0.00	0.00	0.00	1.00	1.20	0.50	2.00	0.40	0.10	1.00
21	0.00	1.20	1.00	0.00	1.24	1.36	0.25	1.50	0.00	0.10	1.00

By applying the improved DBSCAN, the number of clusters and the corresponding parameters are $M = 4$, $E = 0.43$, and $C_{min} = 4$. The specific wind turbine clustering result is shown in Table 9.

Table 9. The clustering result of wind turbines in Case study 3.

Cluster Number	Turbine Number
1	1, 2, 3, 4
2	5, 6, 7, 8, 9, 10, 11, 16, 17, 18, 19, 20
3	12, 13, 14, 15, 21, 22, 23, 24
4	25, 26, 27, 28, 29, 30, 31, 32, 33, 34, 35

Then the improved PSO is used to obtain the parameters of the equivalent wind turbine under faults Z_{f1}. The results of comparing the active and reactive power at the outlet of the original and equivalent wind farm are shown in Figure 13.

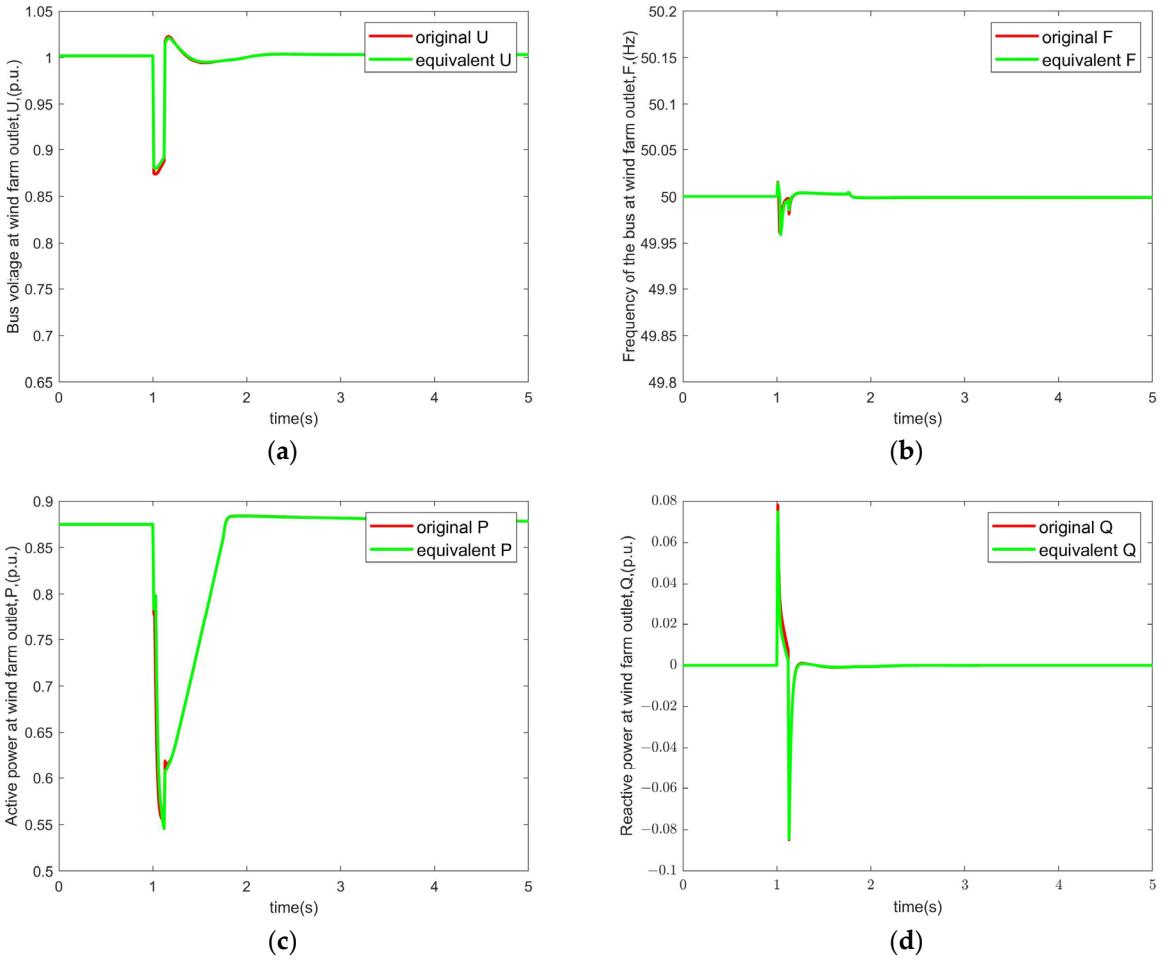

Figure 13. Equivalent results of Case study 3. (**a**) Terminal voltage. (**b**) Active power. (**c**) Reactive power. (**d**) Frequency.

The RMSE of the active and reactive power is 1.22% and 2.46%, respectively. It can be clearly seen that the frequency fluctuation of the bus is very small and cannot cause serious accidents in the grid. From the results, it is clear that the method proposed in this paper is still applicable in large capacity wind farms.

7. Discussion

It is important to notice that the equivalence method proposed in this paper has some limitations. This method is applicable to the case when the turbines in the wind farm have the same structure. This is because the LVRT characteristics of different wind turbines can vary significantly when the model structures of the wind turbines differ greatly. The LVRT characteristics of the wind turbines can vary significantly even when the terminal

voltage drops are the same. At this point, it is not possible to distinguish the difference in LVRT states between different turbines by simply clustering through electrical distance. In this case, it is necessary to combine a variety of clustering indicators and further study a reasonable clustering method.

From Case study 3, it can be seen that this method is also applicable to the equivalent modelling analysis of the LVRT process of a large DFIG wind farm.

8. Conclusions

This paper proposes an LVRT equivalent method for large-scale DFIG wind farms based on PSO and the adaptive DBSCAN. This equivalent method can be applied when the wind turbines in the wind farm have the same structure.

This equivalent model improves the accuracy by considering the influence of static parameters in the wind farm. The existence of errors in the static equivalent can lead to differences between the terminal voltage of the equivalent model and the original wind farm before the fault occurs. However, after the static equivalent, it can significantly improve the similarity between the voltage drops of the equivalent model and the original model during the fault period, which results in similar LVRT characteristics of the wind turbine and thus improves the accuracy of the equivalent model.

The PSO-based dynamic parameter optimization method proposed in this paper is applicable to the LVRT parameter equivalent with discontinuous characteristics. In this method, the basic PSO is improved by changing the initial particles generation method and adaptive change of inertia coefficients. The results show that the improved PSO has higher convergence speed and equivalent accuracy. The DBSCAN-based clustering method proposed in this paper can achieve reasonable clustering of wind turbines. This clustering method can automatically cluster wind turbines by using electrical distance as the clustering index.

The results of the simulations in PSASP show that the obtained equivalent system can approximate the dynamic characteristics of the original wind farm. By comparing the equivalent results with those obtained by the weighted average method and the basic PSO method, it is verified that the proposed equivalent method has a high equivalent accuracy and a fast convergence speed. The system frequency fluctuates only in a small range throughout the equivalence. No serious power system faults are caused by frequency changes. This method can reduce the complexity and increase the speed of the simulation. This method is also applicable to the equivalent modelling analysis of the LVRT process in large DFIG wind farms.

When the model structure of wind turbines in a wind farm is different, the difference in LVRT characteristics between different turbines cannot be shown by clustering only through the electrical distance. In this case, further analysis of reasonable clustering and equivalent methods is needed on this basis.

Author Contributions: Conceptualization, N.Z. and H.M.; Data curation, C.L.; Formal analysis, J.C.; Investigation, Q.F.; Methodology, N.Z.; Project administration, N.Z.; Resources, Z.J.; Software, J.C.; Supervision, H.M.; Validation, Q.F., Z.J. and C.L.; Visualization, N.Z.; Writing—original draft, J.C.; Writing—review & editing, C.L. All authors have read and agreed to the published version of the manuscript.

Funding: This research was funded by State Grid Shandong Electric Power Company under Grant No. 520626220079.

Data Availability Statement: Data are available upon reasonable request to the corresponding author.

Acknowledgments: The financial support from State Grid Shandong Electric Power Company is greatly acknowledged.

Conflicts of Interest: The authors declare no conflict of interest.

References

1. Xie, D.; Hang, Z.; Zheng, F.; Pang, R.; Wan, Y.; Yuan, S.; Zhang, Z. Comparative Analysis of Reserve Configuration of Power System with Storage Considering the Uncertainty of New Energy. In Proceedings of the 2021 IEEE 5th Conference on Energy Internet and Energy System Integration (EI2), Taiyuan, China, 22–24 October 2021; pp. 2490–2495. [CrossRef]
2. Sun, H.; Xu, T.; Guo, Q.; Li, Y.; Lin, W.; Yi, J.; Li, W. Analysis on blackout in great Britain power grid on August 9th 2019 and its enlightenment to power grid in China. *Proc. CSEE* **2019**, *39*, 6183–6191. [CrossRef]
3. Zou, J.; Peng, C.; Xu, H.; Yan, Y. A fuzzy clustering algorithm-based dynamic equivalent modeling method for wind farm with DFIG. *IEEE Trans. Energy Convers.* **2015**, *30*, 1329–1337. [CrossRef]
4. Xue, F.; Song, X.F.; Chang, K.; Xu, T.-C.; Wu, F.; Jin, Y.-Q. Equivalent modeling of DFIG based wind farm using equivalent maximum power curve. In Proceedings of the 2013 IEEE Power & Energy Society General Meeting, Vancouver, BC, Canada, 21–25 July 2013; pp. 1–5. [CrossRef]
5. Liu, Y.; Zhao, D.; Zhang, L.; Zhu, L.; Chen, N. Simulation study on transient characteristics of DFIG wind turbine systems based on dynamic modeling. In Proceedings of the 2014 China International Conference on Electricity Distribution (CICED), Shenzhen, China, 23–26 September 2014; pp. 1408–1413. [CrossRef]
6. Saci, A.; Cherroun, L.; Boudiaf, M. Investigation of Modeling and Control of a Grid Side System based DFIG for a Wind Turbine Machine. In Proceedings of the 2022 19th International Multi-Conference on Systems, Signals & Devices (SSD), Sétif, Algeria, 6–10 May 2022; pp. 315–320.
7. Fu, Y.; Liu, Y.; Huang, L.; Ying, F.; Li, F. Collection System Topology for Deep-Sea Offshore Wind Farms Considering Wind Characteristics. *IEEE Trans. Energy Convers.* **2021**, *37*, 631–642. [CrossRef]
8. Meng, Z.J.; Xue, F.; Chang, K.; Ding, M.; Zhang, J.; Xiang, L.; Shi, J.; Li, X. Applications of an improved equivalent wind method for the aggregation of DFIG wind turbines. In Proceedings of the 2011 4th International Conference on Electric Utility Deregulation and Restructuring and Power Technologies (DRPT), Weihai, China, 6–9 July 2011; pp. 151–155. [CrossRef]
9. Wu, F.; Chen, Y.X.; Gong, G.J.; Shi, L. non-mechanism equivalent model of wind farm for transient stability analysis. In Proceedings of the 2015 5th International Conference on Electric Utility Deregulation and Restructuring and Power Technologies (DRPT), Changsha, China, 26–29 November 2015; pp. 183–186. [CrossRef]
10. Zhao, M.; Wang, Y.; Wang, X.; Chang, J.; Zhou, Y.; Liu, T. Modeling and Simulation of large-scale wind power base output considering the clustering characteristics and correlation of wind farms. *Front. Energy Res.* **2022**, *10*, 237. [CrossRef]
11. Xu, J.; Xue, Y.; Zhang, Q.; Wang, D. A critical review on coherency-based dynamic equivalences. *Autom. Electr. Power Syst.* **2005**, *29*, 91–95.
12. Jin, Y.Q.; Ju, P.; Pan, X.P. Analysis on controller aggregation method for equivalent modeling of DFIG-based wind farm. *Autom. Electr. Power Syst.* **2014**, *38*, 19–24. [CrossRef]
13. Wang, Y.; Lu, C.; Zhu, L.; Zhang, G.; Li, X.; Chen, Y. Comprehensive modeling and parameter identification of wind farms based on wide-area measurement systems. *J. Mod. Power Syst. Clean Energy* **2016**, *4*, 383–393. [CrossRef]
14. Li, W.; Chao, P.; Liang, X.; Ma, J.; Xu, D.; Jin, X. A practical equivalent method for DFIG wind farms. *IEEE Trans. Sustain. Energy* **2017**, *9*, 610–620. [CrossRef]
15. Liu, M.; Pan, W.; Zhang, Y.; Zhao, K.; Zhang, S.; Liu, T. A dynamic equivalent model for DFIG-based wind farms. *IEEE Access* **2019**, *7*, 74931–74940. [CrossRef]
16. Zhao, Z.; Yang, P.; Xu, Z.; Yin, X. Dynamic equivalent modeling of wind farm with double fed induction wind generator based on operating data. In Proceedings of the 2013 5th International Conference on Power Electronics Systems and Applications (PESA), Hong Kong, China, 11–13 December 2013; pp. 1–6. [CrossRef]
17. Sun, T.; Mou, X.; Li, Z. A practical clustering method of DFIG wind farms based on dynamic current error. In Proceedings of the 2015 IEEE Power & Energy Society General Meeting, Denver, CO, USA, 26–30 July 2015; pp. 1–5. [CrossRef]
18. Zhu, L.; Zhang, J.; Zhong, D.; Wang, B.; Wu, Z.; Xu, M.; Li, Q. A study of dynamic equivalence using the similarity degree of the equivalent power angle in doubly fed induction generator wind farms. *IEEE Access* **2020**, *8*, 88584–88593. [CrossRef]
19. Wang, D.; Zhou, Q.; Shen, W.; Gu, D.; Yang, X. Research on Wind Farm Clustering Modeling for Power Grid Dynamic Equivalence. In Proceedings of the 2021 5th International Conference on Smart Grid and Smart Cities (ICSGSC), Tokyo, Japan, 18–20 June 2021; pp. 55–60.
20. Xu, M.; Wang, J.; Zhang, J.A.; Wang, J.; Liu, H.; Wang, G. Wind Farm Multi-Machine Aggregation Equivalent Method based on Probability Clustering. In Proceedings of the 2022 IEEE International Conference on Advances in Electrical Engineering and Computer Applications (AEECA), Dalian, China, 20–21 August 2022; pp. 96–99.
21. Gupta, A.P.; Mitra, A.; Mohapatra, A.; Singh, S.N. A Multi-Machine Equivalent Model of a Wind Farm Considering LVRT Characteristic and Wake Effect. *IEEE Trans. Sustain. Energy* **2022**, *13*, 1396–1407. [CrossRef]
22. Ye, L.; Zhou, J.; Hao, Y.; Yang, X.; Zhou, Y. A Dynamic Equivalent Method for the Offshore Wind Power Farm Based on Operation State. In Proceedings of the 2021 IEEE 1st International Power Electronics and Application Symposium (PEAS), Shanghai, China, 13–15 November 2021; pp. 1–5.
23. Gupta, A.P.; Mohapatra, A.; Singh, S.N. DFIG Equivalence of a Wind Farm by Extended Kalman Filter based Parameters Estimation. In Proceedings of the 2021 9th IEEE International Conference on Power Systems (ICPS), Kharagpur, India, 16–18 December 2021; pp. 1–5.

24. Xu, Y.; Zhang, L.; Wang, N. Study on equivalent model of wind farms with DFIG considering wake effects. *Power Syst. Prot. Control* **2014**, *42*, 70–76.
25. Huang, D.; Zhu, C. Strong Wind Data Augmentation Based on F-DBSCAN and C-SMOTE for Wind Power Forecasting. In Proceedings of the 2021 IEEE 5th Conference on Energy Internet and Energy System Integration (EI2), Taiyuan, China, 22–24 October 2021; pp. 2992–2998.